

EVALUATION OF ERROR PROBABILITIES FOR GENERAL SIGNAL CONSTELLATIONS

Jack W. Stokes, Microsoft Corp., One Microsoft Way, Redmond, WA 98052
jstokes@microsoft.com

James A. Ritcey, Dept. of Electrical Engineering, Box 352500, Univ. of Washington,
Seattle, WA 98195, ritcey@ee.washington.edu

Abstract

Expressions for error probabilities have been derived for commonly used signal constellations such as QAM and MPSK. However, closed form expressions cannot be found for more complex signal constellations such as hexagonally packed signals. Saddle point integration (SPI) has been shown to be an efficient method of evaluating the one dimensional cumulative distribution function (CDF) of a random variable. SPI integrates the moment generating function (MGF) of the test statistic instead of probability density function (PDF). In this paper, the SPI method is used to evaluate P_e for general, complex signal constellations. The first step is to determine the decision regions for each symbol using an algorithm from the graphics literature for calculating Voronoi diagrams. Next, these decision regions are subdivided into subregions that can be evaluated using SPI. The SPI method is very flexible and allows one to model many different system effects such as phase offset, DC offset, and colored noise.

1 Introduction

QAM or MPSK are typically used as the modulation methods for modern digital communication systems. However, from the sampling theory point of view, these modulation schemes are not the most efficient use of the complex baseband area. With continued advances in semiconductors, future communication systems may support more densely packed signal constellations resulting in higher bandwidth efficiency. Expressions for error probabilities have been derived for the commonly used signal constellations such as QAM and MPSK.

However, closed form expressions cannot be found for more complex signal constellations such as hexagonally packed signals. Helstrom [1], [2], [5] and Ritcey [3], [4] demonstrated that saddle point integration (SPI) provides a computationally efficient method for evaluating the one dimensional, cumulative distribution function (CDF) for many different types of probability density functions (PDFs) provided that the Laplace transform of the PDF exists. SPI computes the CDF by integrating the moment generating function (MGF) along a contour in the complex plane instead of integrating the PDF directly. In this paper, the SPI method is extended to two dimensions with arbitrary linear decision regions. With this new method, we evaluate the P_e for general, complex, baseband signal constellations.

An example of a signal constellation which is divided into distinct decision regions for each symbol is given in figure 1. The probability of detection for the l th decision subregion associated with the n th symbol with a priori detection probability a_n is

$$P_d(n, l) = a_n \int_{R_1}^{R_2} \int_{m_1 x_r + b_1}^{m_2 x_r + b_2} p(x_r, x_i) dx_i dx_r. \quad (1)$$

A subregion is defined to have left and right vertical side boundaries located at $x_r = R_1$ and $x_r = R_2$, respectively. The subregion is bounded below by $x_i = m_1 x_r + b_1$ and above by $x_i = m_2 x_r + b_2$. For subregions with no upper (lower) boundary, we set m_2 (m_1) equal to zero and b_2 (b_1) equal to ∞ .

The probability of error for the entire signal constellation with N symbols and L_n subregions for the n th

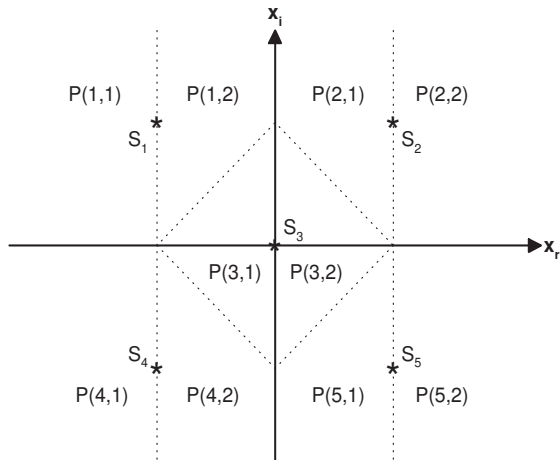


Figure 1: Cross pattern signal constellation with detection regions.

symbol is

$$P_e = 1 - \sum_{n=1}^N \sum_{l=1}^{L_n} P_d(n, l). \quad (2)$$

In order to be practical, the algorithm must accept a set of symbol locations and determine the decision subregions, $P_d(n, l)$, and associated decision boundaries for each symbol. We solve this problem using an algorithm from the graphics literature to construct Voronoi diagrams. Next, these detection regions are subdivided into subregions that can be evaluated using SPI. The SPI method is extremely flexible allowing one to easily model additional system effects such as phase offset, DC offset, and colored noise.

This paper is organized as follows. In section 2, the SPI method is derived for the evaluation of the CDF for complex distributions. In section 3, we discuss the algorithm for determining the decision boundaries. Next, we show how to model the effects of phase and DC offset as well as colored noise in section 4. Finally, we present numerical results in section 5.

2 Saddle Point Integration Within A Subregion

In this section, we derive a method for calculating the detection probability for the l th subregion of the n th symbol. To simplify the equations, we set $P_d = P_d(n, l)$

with the corresponding PDF, $p(x) = p_{n,l}(x)$. Let $h(\mathbf{u}) = E\{\exp(-\mathbf{u}^T \mathbf{x})\}$ be the moment generating function (MGF) of the complex random variable \mathbf{x} written as a random vector, $\mathbf{x} = (x_r \ x_i)^T$,

$$h(u_r, u_i) = \int_{-\infty}^{\infty} \int_{-\infty}^{\infty} p(x_r, x_i) e^{-(u_r x_r + u_i x_i)} dx_r dx_i. \quad (3)$$

P_d can be recovered by the inverse Laplace transform of the MGF.

$$P_d = \int_{s_r - j\infty}^{s_r + j\infty} \int_{s_i - j\infty}^{s_i + j\infty} \frac{h(u_r, u_i)}{u_i} Y(u_r, u_i) \frac{du_i}{2\pi j} \frac{du_r}{2\pi j} \quad (4)$$

where

$$Y(u_r, u_i) = \frac{\psi_1(u_r, u_i)}{u_r + u_i m_2} - \frac{\psi_2(u_r, u_i)}{u_r + u_i m_1} \quad (5)$$

and

$$\begin{aligned} \psi_1(u_r, u_i) &= \Omega_1(u_r, u_i) - \Omega_2(u_r, u_i) \\ \psi_2(u_r, u_i) &= \Omega_3(u_r, u_i) - \Omega_4(u_r, u_i) \\ \Omega_1(u_r, u_i) &= \exp(u_r R_2 + u_i (R_2 m_2 + b_2)) \\ \Omega_2(u_r, u_i) &= \exp(u_r R_1 + u_i (R_1 m_2 + b_2)) \\ \Omega_3(u_r, u_i) &= \exp(u_r R_2 + u_i (R_2 m_1 + b_1)) \\ \Omega_4(u_r, u_i) &= \exp(u_r R_1 + u_i (R_1 m_1 + b_1)). \end{aligned} \quad (6)$$

The complex, normal PDF with mean, \mathbf{M} , and covariance, \mathbf{K} , is

$$p(x_r, x_i) = \frac{1}{\sqrt{4\pi^2 |\mathbf{K}|}} e^{-\frac{1}{2}(\mathbf{x} - \mathbf{M})^T \mathbf{K}^{-1} (\mathbf{x} - \mathbf{M})}. \quad (7)$$

Inserting (7) into (3), completing the square and integrating yields the following MGF for a complex, normal random variable,

$$h(\mathbf{u}) = \exp(-\mathbf{m}^T \mathbf{u} + \frac{1}{2} \mathbf{u}^T \mathbf{K} \mathbf{u}). \quad (8)$$

It can be shown that the integrand of (4) is a two dimensional, convex \cup function. Therefore, the integrand has a minimum at the saddle point location $\mathbf{s} = (s_r, s_i)^T$. Thus for $\Re(u_i) < 0$, $\mathbf{s} = \text{argmin}(\Phi(\mathbf{u}))$ where the phase, $\Phi(\mathbf{u})$, is given by

$$\exp(\Phi(\mathbf{u})) = \frac{h(u_r, u_i)}{u_i} Y(u_r, u_i). \quad (9)$$

The saddle point can be computed using a simple multi-dimensional least mean squares algorithm

$$\mathbf{s}^{new} = \mathbf{s}^{old} - \mu \nabla_{\mathbf{u}} \Phi(\mathbf{u})|_{\mathbf{s}^{old}} \quad (10)$$

where μ is the step size, and $\nabla_{\mathbf{u}}$ is the gradient with respect to \mathbf{u} . The first partial derivatives of $\Phi(\mathbf{u})$ required for the calculation of the gradient in (10) are

$$\begin{aligned} \frac{\partial}{\partial u_r} \Phi(u_r, u_i) &= \frac{\partial}{\partial u_r} \ln(h(u_r, u_i)) + \frac{\partial}{\partial u_r} \ln(Y(u_r, u_i)) \\ \frac{\partial}{\partial u_i} \Phi(u_r, u_i) &= \frac{\partial}{\partial u_i} \ln(h(u_r, u_i)) - \frac{1}{u_i} + \frac{\partial}{\partial u_i} \ln(Y(u_r, u_i)) \end{aligned}$$

where

$$\begin{aligned} \frac{\partial}{\partial u_r} \ln(Y(u_r, u_i)) &= \frac{R_2 \Omega_1(u_r, u_i) - R_1 \Omega_2(u_r, u_i)}{Y(u_r, u_i)(u_r + u_i m_2)} \\ &- \frac{\psi_1(u_r, u_i)}{Y(u_r, u_i)(u_r + u_i m_2)^2} \\ &- \frac{R_2 \Omega_3(u_r, u_i) - R_1 \Omega_4(u_r, u_i)}{Y(u_r, u_i)(u_r + u_i m_1)} \\ &+ \frac{\psi_2(u_r, u_i)}{Y(u_r, u_i)(u_r + u_i m_1)^2} \end{aligned}$$

and

$$\begin{aligned} \frac{\partial}{\partial u_i} \ln(Y(u_r, u_i)) &= \\ &- \frac{m_2 \psi_1(u_r, u_i)}{Y(u_r, u_i)(u_r + u_i m_2)^2} \\ &+ \frac{(R_2 m_2 + b_2) \Omega_1(u_r, u_i) - (R_1 m_2 + b_2) \Omega_2(u_r, u_i)}{Y(u_r, u_i)(u_r + u_i m_2)} \\ &- \frac{(R_2 m_1 + b_1) \Omega_3(u_r, u_i) - (R_1 m_1 + b_1) \Omega_4(u_r, u_i)}{Y(u_r, u_i)(u_r + u_i m_1)} \\ &+ \frac{m_1 \psi_2(u_r, u_i)}{Y(u_r, u_i)(u_r + u_i m_1)^2}. \end{aligned}$$

Rewriting (4) in terms of the phase, the P_d is given by

$$P_d = \int_{s_i - j\infty}^{s_i + j\infty} \int_{s_r - j\infty}^{s_r + j\infty} \exp(\Phi(\mathbf{u})) \frac{du_r}{2\pi j} \frac{du_i}{2\pi j}. \quad (11)$$

Extending the results from Schwartz [13] and Rice [9], trapezoidal integration is used to numerically evaluate the multidimensional integral in (11)

$$P_d = \lim_{\Delta u_r \rightarrow 0, \Delta u_i \rightarrow 0} F(\mathbf{u}, \Delta \mathbf{u}) \quad (12)$$

where

$$F(\mathbf{u}, \Delta \mathbf{u}) = \frac{-\Delta u_r \Delta u_i}{4\pi^2} \sum_{l_i=-L_i}^{L_i} \sum_{l_r=-L_r}^{L_r} e^{\Phi(\mathbf{u})} + E_T(\Delta \mathbf{u}), \quad (13)$$

$u_k = s_k + j l_k \Delta u_k$, Δu_k is the step size along the k th axis, and L_k provides the number of steps required to achieve a result that is within the desired error tolerance. Evaluation of (12) produces two sources of error due to finite step sizes and the truncation error. The truncation error, $E_T(\Delta \mathbf{u})$, results from truncating the integral computation at L_k and is also a function of the step size.

Extending the results from Rice [10] provides an initial estimate for the step size

$$\Delta u_k = \sqrt{2 / \frac{\partial^2}{\partial u_k^2} \Phi(\mathbf{s})} \quad (14)$$

for $k \in \{r, i\}$. The CDF is computed by halving the step size in each dimension until the result converges to the desired error tolerance. An algorithm for computing the multidimensional sum in (12) is given by Kohn [6].

3 Voronoi Diagrams

The first step to calculating the P_e for the signal constellation is to determine all decision regions for each symbol. Once the decision regions are known, the SPI method outlined in the previous section can be used to calculate $P_d(n, l)$. The problem of determining the detection boundaries for general signal constellations is identical to computing the Voronoi diagram for a set of two dimensional vertices in computer graphics. The Voronoi diagram is the dual of Delaunay triangulation which is a popular method for generating triangular meshes. Therefore, much research has been devoted to this problem and several efficient algorithms have been developed. We choose to use an algorithm developed by Steven Fortune because it computes the results based on the entire set of 2-D vertices as opposed to other algorithms which begin with 3 vertices containing all other vertices. Software which implements the algorithm can be found at <http://netlib.org/voronoi/index.html>.

4 Phase and DC Offset, Colored Noise

The SPI method allows one to consider the effects of various system problems such as phase offset, DC offset, and colored noise on the error probability. Phase offset results from the inability of the receiver to perfectly estimate the symbol's phase. The result is a rotation of the signal constellation. By applying a rotation to the mean of each symbol in the signal constellation, we can easily evaluate phase errors.

While phase offset results in a rotation of the signal constellation, DC offset corresponds to a two dimensional translation error. DC offset can be introduced by a DC bias in the analog components of the transmitter or receiver. Like the phase offset, DC offset can be modeled by applying a two dimensional translation to the mean of each symbol.

The detection boundaries in the receiver are fixed assuming that the received signal constellation does not have either phase or DC offset. Thus, the detection boundaries computed by the Voronoi diagram method must be computed before the phase and DC offsets are applied to the signal constellation.

Error probabilities are usually estimated for a model assuming additive white Gaussian noise (AWGN). However, in practice the noise is often colored due to effects of the transmission medium or linear filters operating on white noise. For the SPI method, the effects of colored noise can be evaluated by setting the covariance matrix for each symbol to something other than the identity matrix.

5 Numerical Results

In this section, we compare error probabilities for 16-ary QAM and a 16-ary hexagonal signal constellation including the effects of phase offset, DC offset, and colored noise. The 16-ary QAM signal constellation has symbols located at $S(i,q)$ where $i, j \in \{-3, -1, 1, 3\}$. The 16-ary hexagonal signal constellation is shown in figure 2. For this constellation, the symbols are located at $S(i, q) = S_1 + (s, \sqrt{3}t)$ where s and t are integers and S_1 is located at $(0, 2/\sqrt{3})$. For all systems, the desired error tolerance is $10e-7$. In figure 3, we compare error probabilities for the QAM and hexagonal signal

constellations for AWGN, phase offset, DC offset, and colored noise, respectively. For both constellations, the phase rotation examples introduce a phase offset of +10 degrees, the DC offset examples add a linear translation of $(0.15, 0.15)$, and the colored noise examples are modeled with a covariance matrix, K , of

$$K = \begin{bmatrix} 1.25 & 0.25 \\ 0.25 & 0.75 \end{bmatrix}. \quad (15)$$

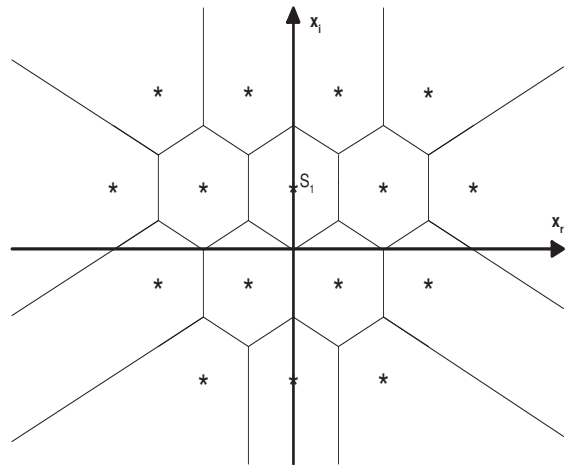


Figure 2: 16-ary hexagonal signal constellation.

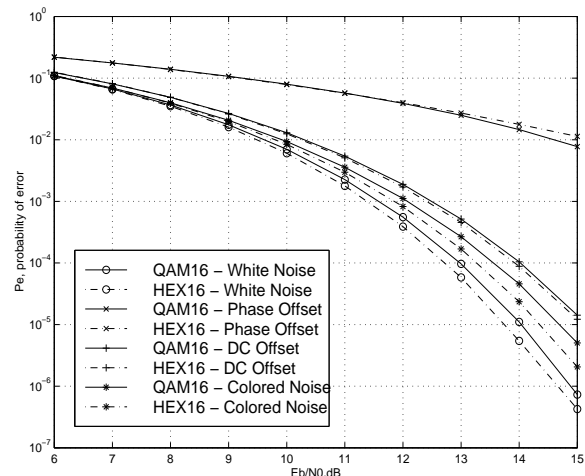


Figure 3: P_e vs. E_b/N_0 for 16-ary QAM and hexagonal signal constellation with AWGN, +10 degree phase offset, $(0.15, 0.15)$ translation and colored noise.

As expected, the results in figure 3 shows that the AWGN system offers better performance than any of

the other systems for both the hexagonal signal constellation (HSG) and QAM. The HSG results for AWGN show an improvement in the E_b/N_0 of 0.25 dB for $P_e = 10e - 5$. Likewise, the results for the case of colored noise show a similar improvement in the E_b/N_0 of 0.4 dB for the HSG at $P_e = 10e - 5$. In addition, both signal constellations perform about 0.5 dB worse for colored noise than for AWGN. However for the DC offset case, the hexagonal signal constellation offers only a slight improvement over QAM. With DC offset, the HSG and QAM perform worse by 1.50 and 1.25 dB, respectively, in E_b/N_0 when compared with AWGN for $P_e = 10e - 5$. Finally for the case of phase offset, QAM constellation actually performs better than the hexagonal signal constellation for $E_b/N_0 > 12$ dB. In addition, both signal constellations with phase offset perform significantly worse than for AWGN, colored noise, or DC offset.

6 Conclusions

In this paper, we have derived a method to evaluate error probabilities for general signal constellations. This method is based on multivariate Saddle Point Integration and an algorithm used to calculate Voronoi diagrams. Using this method, we evaluated error probabilities for 16-ary QAM and a 16-ary hexagonal signal constellation. When considering densely packed signal constellations, we have shown it is important to characterize the system effects for the receiver and transmission medium including phase offset, DC offset, and colored noise. The system designer must then evaluate the error probability associated with each of these effects and determine if the performance of the proposed constellation justifies the increased complexity of the transmitter and receiver. Although the hexagonal signal constellation performs better than 16-ary QAM under most conditions, it is more susceptible to extreme phase rotation. Saddle Point Integration offers a general and efficient method for evaluating all of these effects for any signal constellation.

References

[1] C. W. Helstrom, *Approximate evaluation of detection probabilities in radar and optical communication*

tions, IEEE Trans. Aero. & Elect. Sys., 14 (1978), pp. 630-640.

[2] C. W. Helstrom, *Evaluating the detectability of gaussian stochastic signals by steepest descent integration*, IEEE Trans. Aero. & Elect. Sys., 19 (1983), pp. 428-437.

[3] C. W. Helstrom and J. A. Ritcey, *Evaluating radar detection probabilities by steepest descent integration*, IEEE Trans. Aero. & Elect. Sys., 20 (1984), pp. 624-633.

[4] C. W. Helstrom and J. A. Ritcey, *Evaluation of the noncentral F-distribution by numerical contour integration*, SIAM J. Sci. Stat. Comput., 6 (1985), pp. 505-514.

[5] C. W. Helstrom, *Calculating error probabilities for intersymbol and cochannel interference*, IEEE Trans. Commun., COM-34, 5 (1986), pp. 430-435.

[6] R. Kohn, *Nesting do loops to any depth*, J. Stat. Comput. Simul., 4 (1981), pp. 41-45.

[7] R. Lugannani and S. O. Rice, *Saddle point approximation for the distribution of the sum of independent random variables*, Adv. Appl. Prob., 12 (1980), pp. 475-490.

[8] D. B. Owen, *Orthant probabilities*, Encyclopedia of Stat. Science, ed. S. Kotz & N.L. Johnson, 6 (1985), pp. 521-523.

[9] S.O. Rice, *Efficient evaluation of integrals of analytic functions by the trapezoidal rule*, Bell Sys. Tech. Journal, 52 (1973), pp. 707-723.

[10] S.O. Rice, *Distribution of quadratic forms in normal random variables - evaluation by numerical integration*, SIAM J. Sci. Stat. Comput., 1 (1980), pp. 438-448.

[11] C. Rivera, *Analysis of communication systems using the method of saddle point integration*, Ph.D. Dissertation, Dept. of Electrical Engineering, Univ. of Washington, Seattle, WA, 1995.

[12] C. Rivera and J. A. Ritcey, *Error probabilities for QAM systems on partially coherent channels with intersymbol interference and crosstalk*, IEEE Trans. Commun., COM-46, 6 (1998), pp. 775-783.

[13] C. Schwartz, *Numerical integration of analytic functions*, J. Comput. Physics, 4 (1969), pp. 19-29.